Mod Pathol 38 (2025) 100635

MODERN PATHOLOGY

USCAP UNITED STATES AND CANADIAN ACADEMY OF PATHOLOGY
Creating a Better Pathologist

Journal homepage: https://modernpathology.org/

Research Article

GLI1-Altered Mesenchymal Tumor—Multiomic Characterization of a Case Series and Patient-Level Meta-analysis of One Hundred Sixty-Seven Cases for Risk Stratification

Maximus C.F. Yeung[a,*], Anthony P.Y. Liu[b,c,d], Sio-In Wong[e], Herbert H. Loong[f,g], Tony W.H. Shek[a]

[a] *Department of Pathology, School of Clinical Medicine, The University of Hong Kong, Hong Kong;* [b] *Department of Paediatrics and Adolescent Medicine, School of Clinical Medicine, The University of Hong Kong, Hong Kong;* [c] *Department of Paediatrics and Adolescent Medicine, Hong Kong Children's Hospital, Hong Kong;* [d] *Division of Haematology and Oncology, The Hospital for Sick Children, Toronto, Canada;* [e] *Department of Anatomic Pathology, Centro Hospitalar Conde de São Januário, Macau, People's Republic of China;* [f] *Department of Clinical Oncology, The Chinese University of Hong Kong, Hong Kong;* [g] *State Key Laboratory in Translational Oncology, The Chinese University of Hong Kong, Hong Kong*

ARTICLE INFO

Article history:
Received 3 July 2024
Revised 2 September 2024
Accepted 6 October 2024
Available online 21 October 2024

Keywords:
GLI1
GLI1 altered
mesenchymal tumor
soft tissue tumor
risk stratification

ABSTRACT

GLI1-altered mesenchymal tumors have recently emerged as a distinctive group of neoplasms characterized by *GLI1* fusions or amplifications. Although there is clearly metastatic potential, the clinicopathologic features predicting for metastasis are currently unknown. Herein, we present 6 cases of *GLI1*-altered mesenchymal tumors with multiomics analysis. The median patient age was 50 years (range, 3-68 years). They arose from the extremities and trunk (2/6), head and neck region (2/6), and gastrointestinal tract (2/6). Histologically, they featured uniform round to ovoid cells with nested architecture and a rich vascular network. One case displayed abundant multinucleated giant cells. All stained positive for GLI1 (5/5) and CD56 (6/6). Molecularly, they featured *GLI1* fusion (5/6) and amplification (1/6). Fusion partners included *ACTB* (3/5), *TXNIP* (1/5), and novel *TUBA1B* (1/5). Multiomics analysis revealed they possessed distinct expression and epigenomic profiles. All the 6 cases had follow-up information, with 5 of them having no evidence of disease at a median follow-up of 30 months (range, 17.3-102 months), and 1 case being died of disease with regional neck lymph node and bilateral lung metastasis at 81.5 months of follow-up. By incorporating cases reported in the literature, we analyzed clinicopathologic features of a total of 167 cases predictive of malignant behavior. We found that size $\geq$6 cm and mitotic count $\geq$5 per 10 high-power fields are predictive of metastasis. Cases with both high-risk features had significantly poorer survival. This study expands the literature database of *GLI1*-altered mesenchymal tumors and identifies features that can be used for risk stratification.

Introduction

GLI1-altered mesenchymal tumors represent an emerging molecularly defined group of tumors characterized by either *GLI1* fusion or amplification. The diverse anatomical distribution and variable clinical behavior of these tumors present challenges in their diagnosis and management. Originally described to be found predominantly in the head and neck (H&N) regions, they are subsequently found in much wider anatomical locations, such as trunk and extremities, gastrointestinal tracts, and genitourinary tracts. Although there is clear evidence of metastatic

* Corresponding author.
E-mail address: mcfyeung@hku.hk (M.C.F. Yeung).

0893-3952/$ - see front matter
https://doi.org/10.1016/j.modpat.2024.100635

potential from different case reports and series, the clinicopathologic features predicting malignant behavior are currently unknown.

In this study, we report an additional 6 cases of *GLI1*-altered mesenchymal tumors with multiomics analysis. By integrating cases from a comprehensive literature review with our cohort, we aim to identify clinicopathologic features predictive of metastasis and derive risk stratification factors for *GLI1*-altered mesenchymal tumors.

Materials and Methods

Case Series

The current case series was retrieved from the archived or consultation files from collaborating hospitals. The clinicopathologic information was extracted from electronic patient records. The study was approved by local institutional review board.

Literature Review

Cases of *GLI1*-altered soft tissue tumors published in English literature on or before August 31, 2024, were retrieved on PubMed and Google Scholar search using keywords "GLI1," "GLI1-altered," "GLI1-fusion," "GLI1 amplified," "Soft tissue tumor," and "Mesenchymal tumor." Plexiform fibromyxoma and gastroblastoma were excluded. All the clinicopathologic and molecular parameters available in the publication or supplementary information were extracted.

Targeted RNA Sequencing and Analysis

RNA was extracted from the formalin-fixed paraffin-embedded (FFPE) tissue. RNA was subjected to Illumina Pan-Cancer RNA sequencing panel. The library prepared was sequenced by NextSeq 500/550 mid-output v.2 kit on NextSeq 500 sequencer (Illumina) or MiniSeq high-output kit on MiniSeq sequencer (Illumina) at 76-bp pair-end reads. The raw reads were aligned to reference human genome (hg38) by STAR v.2.7.7.[1] The fusion transcripts were determined by STAR Fusion software v.1.9.1[1] and Arriba v2.1.[2] Gene expression profiles were determined and compared with other tumor types sequenced under the same panel using the R Bioconductor package DESeq2.[3]

DNA Extraction

Four cases had additional tissue sections available for whole-exome sequencing (WES) and methylation EPIC array analysis. Genomic DNA was extracted from FFPE tissue using the QIAamp DNA FFPE Advanced Kit (Qiagen).

Whole-Exome Sequencing

Library preparation and Illumina sequencing (pair-end sequencing of 151 bp) were performed at The University of Hong Kong, LKS Faculty of Medicine, Centre for PanorOmic Sciences, and Genomics Core. Briefly, the libraries were prepared using the xGen cfDNA & FFPE DNA Library Prep v2 MC Kit, followed by FFPE-repairing procedure using the NEBNext FFPE DNA Repair Mix v2. Exome capture was prepared based on the protocol of IDT xGen hybridization capture of DNA libraries for next-generation sequencing target enrichment. The enriched libraries were validated by Fragment Analyzer and Qubit for quality control analysis. Illumina NovaSeq 6000 was used for pair-end 151-bp sequencing.

Whole-Exome Sequencing Data Analysis

The exome sequencing reads after quality control were aligned to the hg38 Gencode V36 reference sequence with Burrows-Wheeler Aligner (bwamem, v0.7.17).[4] PCR duplicates were marked by Picard (v2.18.11), and the BAM files were then indexed by Samtools (v1.9). Base quality score recalibration was performed by the BaseRecalibrator and ApplyBQSR tools from the Genome Analysis Toolkit (GATK, v4.4)[5] according to GATK best practices. Somatic variants including single-nucleotide variants and small indels were detected using Mutect2 in GATK on processed exome data of tumor and matched nontumor normal samples. Annotation of variants was performed by Annovar (v2019/04) on the Refseq gene model.[6] Variants with variant allele fraction $\geq$5% in the coding and splice site regions were included for analyses. The variants were classified according to the AMP/ASCO/CAP standards and guidelines for interpretation and reporting sequence variants in cancer.[7] Copy number variation was according to GATK pipeline. Microsatellite instability status was called using MSI-sensor-pro.[8] Tumor mutational burden was determined by maftools.[9]

DNA Methylation–Based Classification

Methylation analysis was performed using Infinium Methylation EPIC V2 BeadChips (Illumina). Raw signal intensities were obtained from IDAT files of samples using the minfi Bioconductor package version 1.34.0.[10] Unprocessed IDAT files from selected entities of the methylation profiling classifier developed by the German Cancer Research Center (Deutsches Krebsforschungszentrum, DKFZ) were used as a reference.[11] Data sets from Illumina EPIC V2, EPIC V1, and 450k samples were merged using the combineArrays function in minfi. After probe-filtering criteria were applied according to the GitHub repository, unsupervised nonlinear dimension reduction was performed using the 10,000 most variable probes (according to mean absolute deviation) among combined samples. The t-distributed stochastic neighbor embedding (t-SNE) plots for the 4 cases of *GLI1*-altered tumors and selected entities of reference samples were made using the Rtsne package (version 0.15).

Statistical Analysis

All statistical analyses were performed in R. In the analysis of different prognostic factors, categorical variables were compared using the Fisher exact test, whereas continuous variables were analyzed by the Wilcoxon rank sum test. Univariate and multivariate logistic regression analyses were performed to investigate factors associated with metastasis. The survival Kaplan-Meier curve was plotted using the R Bioconductor package survminer, and statistical significance was measured using the log-rank test. $P < .05$ was considered significant.

Results

Clinical Features

The clinicopathologic characteristics of the 6 cases in the study cohort are presented in Table 1. The median age was 50 years (range, 3-68 years). The average tumor size was 5.8 cm (range, 2.5-10 cm). The tumors were present in 4 men and 2 women. They were in the trunk and extremities (2/6), H&N region (2/6), and gastrointestinal tract (2/6). All the cases had follow-up information, with 5 cases having no evidence of diseases after a median of 30-month follow-up (range, 17.3-102 months), whereas 1 died of disease after 81.5 months with regional lymph nodes and bilateral lung metastasis.

Histologic Features

Histologically, they featured multilobulated architecture at a lower power (Fig. 1A). Some of them had cystic changes and myxoid stroma (Fig. 1B). They were composed of uniform round to ovoid tumor cells forming trabeculae, small sheets, or clusters among fine fibrovascular septa. The tumor cells possessed monomorphic nuclei with fine to stippled chromatin, inconspicuous to small nucleoli, and a moderate amount of clear cytoplasm (Fig. 1C). Some areas feature more spindle morphology with bland nuclei (Fig. 1D). One case displayed a large number of multinucleated giant cells (Fig. 1E). Protrusion into vascular space was also evident (Fig. 1F). Mitotic figures ranged from 0 to 15 per 10 high-power fields (HPFs).

Immunohistochemistry

The immunohistochemistry (IHC) results of the current cohort are summarized in Table 1. All the tested cases were positive for GLI1 (4/4), CD56 (5/5), and cyclin D1 (4/4) (Fig. 2A, B). Some were positive for SMA (3/6) and CD10 (2/3) (Fig. 2C). All the tested cases were consistently negative for AE1/3 (0/6), CAM5.2 (0/5), CD34 (0/6), and STAT6 (0/4). One case (case 2) showed diffuse nuclear staining for BCOR (Fig. 2D), which led to the initial misdiagnosis as sarcoma with *BCOR* genetic alteration. Fluorescence in situ hybridization performed was negative for *BCOR* translocation.

Molecular Features

Molecularly, all the cases had *GLI1* gene alteration by definition and are demonstrated by RNA sequencing and/or fluorescence in situ hybridization (Supplementary Fig. S1), with 5 having *GLI1* translocation and 1 having *GLI1* amplification. The fusion partners included *ACTB* (3/5), *TXNIP* (1/5), and *TUBA1B* (1/5). The *TUBA1B* partner had not been reported in the literature previously (Fig. 3A).

RNA-Seq Analysis

Differential gene expression analysis was performed comparing *GLI1*-altered mesenchymal tumors with other tumors sequenced with the same targeted panel, such as Ewing sarcoma and dermatofibrosarcoma protuberans. As expected, the expression of *GLI1* gene and the effector genes of the GLI1 protein in the sonic Hedgehog signaling pathway such as the *PTCH1* gene was significantly higher in *GLI1*-altered tumors compared with other non-*GLI1*−altered tumors (Fig. 3B, C). By clustering analysis through t-SNE plots and hierarchical clustering (Fig. 3D, E), *GLI1*-altered mesenchymal tumors form a distinct cluster, signifying they have a distinct expression profile.

Whole-Exome Sequencing

Four cases have additionally undergone WES. No clinically relevant (AMP/ASCO/CAP guidelines tiers I and II)[7] single-nucleotide variants or short insertion deletion was detected. All the sequenced cases were microsatellite stable with low tumor mutational burden (ie, <10 mutations/Mb). As expected, the case with *GLI1* amplification featured amplification of *MDM2*, *CDK4*, and *DDIT3* genes, which were adjacent to the *GLI1* gene.

Methylation EPIC Profiling

We investigated if *GLI1*-altered mesenchymal tumors have distinct methylation profiling. By unsupervised clustering analysis with DKFZ reference cohort through t-SNE plot, they form a distinct cluster from other entities that may come into differential diagnosis, such as myopericytoma, clear cell sarcoma, and various round cell sarcomas (eg, Ewing sarcoma and BCOR-rearranged sarcoma) (Fig. 4). They are closest to but well separated from well-differentiated liposarcoma and dedifferentiated liposarcoma characterized by *MDM2* gene amplification, which can also occur in *GLI1*-amplified tumors.[12]

Literature Review and Risk Stratification

A literature review identified 161 reported cases of *GLI1*-altered mesenchymal tumors from 38 publications,[13-50] bringing the total number of cases to 167. Considering all cases with molecular confirmation (n = 163), the average patient age was 40.6 years (range, 0-88 years). The male:female ratio was 1.17:1. The average tumor size was 5.3 cm (range, 0.6-21.2 cm). Tumors most commonly arose in the trunk and extremities (48.8%), followed by the H&N (28.1%), intraabdominal (15%), pelvic (5.6%), intrathoracic (1.9%), and rare intracranial regions (0.6%). The intraabdominal region encompassed the gastrointestinal tract (75%), kidney (12.5%), and retroperitoneum (12.5%), whereas pelvic organs included the ovary and uterus. There were 25.8% cases showing metastasis, the most common sites being the lungs (48%), regional lymph nodes (36%), and peripheral soft tissue sites (28%). Nearly half of the metastatic cases (48%) had multiple metastatic sites. Most of the cases exhibited *GLI1* fusion (66.3%); the remaining displayed *GLI1* amplification (32.5%) and rarely both fusion and amplification (1.2%). For those characterized by *GLI1* fusion, the most common fusion partner is the *ACTB* gene (58.3%), followed by *MALAT1* (11.7%) and *PTCH1* (7.8%). Rare fusion partners included *AARS*,[25] *APOD*,[32] *DDIT3*,[25] *DERA*,[35] *FOXO4*,[18,39] *HNRNPA1*,[38] *NCOR2*,[31] *NEAT1*,[38] *PAMR1*,[41] *ADAMTSL2*,[38] *SRGN*,[23] *RP11-306J24.5*,[38] *SYT*,[31] *MRTFA*,[50] *TXNIP*,[38] *TUBA1A*,[47] and a novel *TUBA1B* in our series. The fusion breakpoint of the *GLI1* gene was mainly in exon 6 (48.6%), exon 5 (22.9%), and exon 7 (11.4%). Other locations, including exon 4, exon 2, exon 9, intron 5, and intron 4, had also been reported.

Apart from GLI1 IHC staining, which was reported to be highly sensitive to specific markers,[51] stainings that are more frequently expressed include CD56 (71/77), CD10 (34/38), and

Table 1
Summary of clinicopathologic and molecular features of current cohort

Patient	Age (y)	Sex	Site	Size (cm)	Morphology	GLI1 alterations	Mitoses (per 2 mm^2)	Necrosis	LVI	Positive IHC	Negative IHC	Follow-up (mo)
1	3	M	Stomach	3.5	Multilobulated, anastomosing cord, cystic changes, rich capillary network, oval to spindle cells, and no definite biphasic component	TUBA1B (ex1)::GLI1 (ex6)	15	No	No	SMA (f), CD56 (p), cyclin D1, vimentin, MNF116 (p, m), BCL2, TLE1, glypican-3 (f), GLI1	S100, AE1/3, CAM5.2, Syn, EMA, desmin, h-caldesmon, c-kit, DOG-1, CD31, HMB45, melan A, NSE, Oct3/4, SALL4, AFP, BCOR, CD34, SATB2, pan-TrK, SDH-B (preserved)	NED (102)
2	50	M	Right forearm	9.5	Multilobulated, oval to spindle cell, bland nuclei, myxoid stroma, and abundant multinucleated giant cells	ACTB (ex1)::GLI1 (ex6)	1	No	No	BCOR, TLE, SATB2, BCL2, SMA, CD56, cyclin D1, CD99, GLI1	S100, SOX10, AE1/3, CAM5.2, Syn, Cg, desmin, myosin, STAT6, CD34, EMA, MUC4, HMB45, melan A, pan-Trk, INI1 (preserved), SMARCA4 (preserved); beta-catenin cytoplasmic	NED (32.3)
3	13	M	Left tongue	2.5	Multilobulated, uniform ovoid to epithelioid cells with rich delicate fibrovascular network, bland nuclei, and PNI+	Amplification, RNA-seq negative	7	No	Yes	CD56, CDK4, GLI1, GATA3 (w, f), CD68 (w, f), S100 (w, f), SOX10 (w, f), Syn (w, f), CD10 (w, f), CD99 (w, f)	CK8/18, p63, p40, 34betaE12, desmin, c-kit, myogenin, GFAP, ERG, HMB45, SMA, AE1/3, Cg, EMA, STAT6, CD34	NED (19)
4	68	F	Right floor of mouth	4.1	Uniform round to ovoid cells in trabeculae, small sheets, or clusters; bland nuclei; and moderate amount of clear cytoplasm	ACTB (ex1)::GLI1 (ex2)	0	No	No	Vimentin, c-kit (f, w), p16 (f), CD56, cyclin D1, EMA	p63, PAX8, MSA, desmin, melan A, HMB45, DOG-1, CD31, ERG, NSE, TFE3, CD68, S100, SMA, AE1/3, CAM5.2, Syn, Cg, CD10, CD34	DOD (81.5)
5	66	F	Small bowel	10	Monotonous round to epithelioid cells arranged in nests, sheets, cords, and trabeculae in a vascularized stroma	TXNIP (ex2)::GLI1 (ex6)	3	Focal	No	Vimentin (f), NSE (f), SMA, EMA	S100, SOX10, AE1/3, CDK4, MDM2, STAT6, CD34, claudin-4, GATA-3, D2-40, melan A, HMB45, c-kit, DOG-1, desmin, calponin, myogenin, SALL-4, arginase-1, AFP, glypican-3, OCT3/4, ERG, TRK, inhibin, SF-1, NUT, BCOR, CD30, LCA, CD3, CD20, ALK-1, GLI1, beta-catenin (cytoplasmic); INI-1, SMARCA2, SMARCA4, and ARID1A are preserved	NED (30.2)
6	54	M	Right calf	5.5	Uniform polygonal cells in small nests, ribbons, and interconnected cords with rich fine delicate capillary network and myxoid stroma	ACTB (ex2)-GLI1 (ex6)	<1	No	No	Fli-1, vimentin and claudin-1, p16 (p)	Collagen IV, claudin 4, WT1, SMMS1, calponin, caldesmon, desmin, CD146, PDGFRB, CDK-4, MDM2	NED (17.3)

DOD, died of disease; (f), focal; IHC, immunohistochemistry; LVI, lymphovascular invasion; (m), moderate; NED, no evidence of disease; (p), patchy; (w), weak.

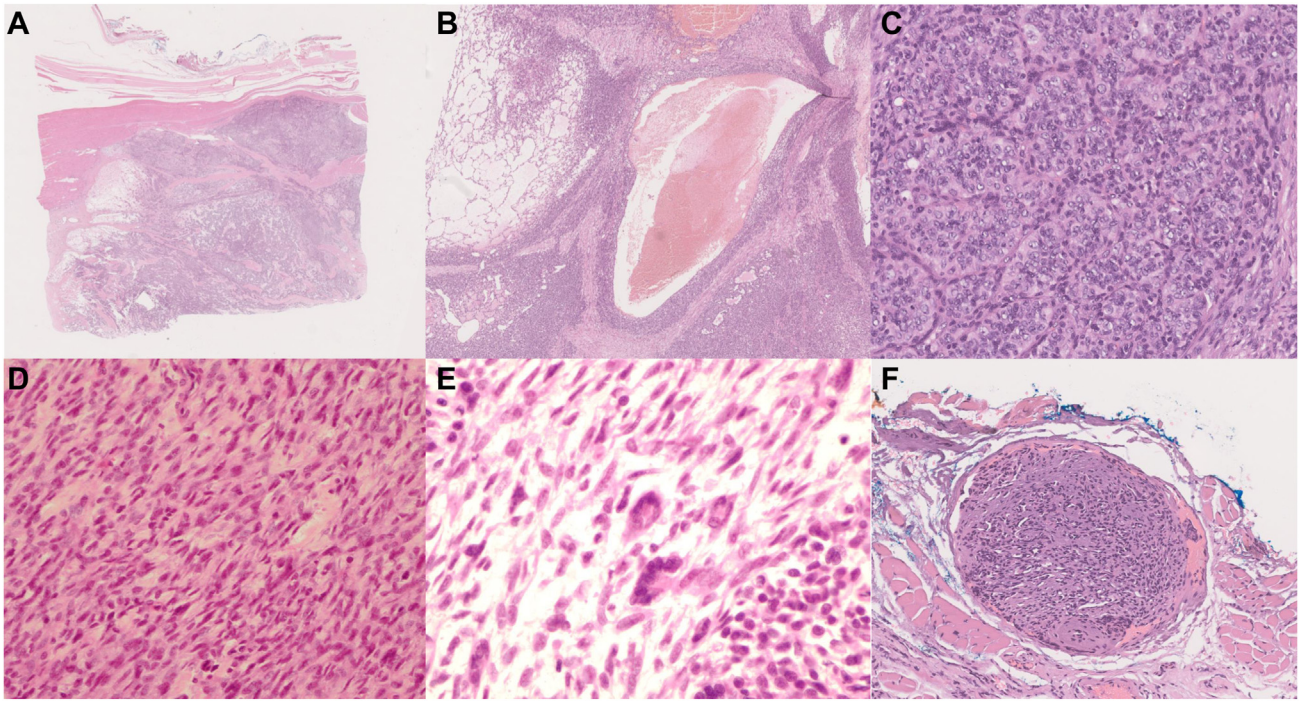

Figure 1.
Histologic features of *GLI1*-altered mesenchymal tumors. (A) They featured multilobulated architecture at a lower power. (B) Some of them had cystic changes and myxoid stroma (case 1). (C) They were composed of uniform round to ovoid tumor cells forming trabeculae, small sheets, or clusters among fine fibrovascular septa. The tumor cells possessed monomorphic nuclei with fine to stippled chromatin, inconspicuous to small nucleoli, and a moderate amount of clear cytoplasm. (D) Some cases displayed spindle cell morphology with bland nuclei. (E) One case (case 2) displayed many multinucleated giant cells. (F) Protrusion into vascular space was also evident.

cyclin D1 (24/24). Some of them also express S100 (56/130), SMA (39/119), and AE1/3 (29/90) (Supplementary Table S1).

We then investigated if there were any differences in clinicopathologic features between *GLI1* fusion and *GLI1*-amplified tumors. Compared with *GLI1* fusion tumors, *GLI1*-amplified tumors had a smaller size, were more common in extremities, and had a higher mitotic index (Table 2). Intraabdominal tumors mainly harbored fusion instead of amplification. There was no

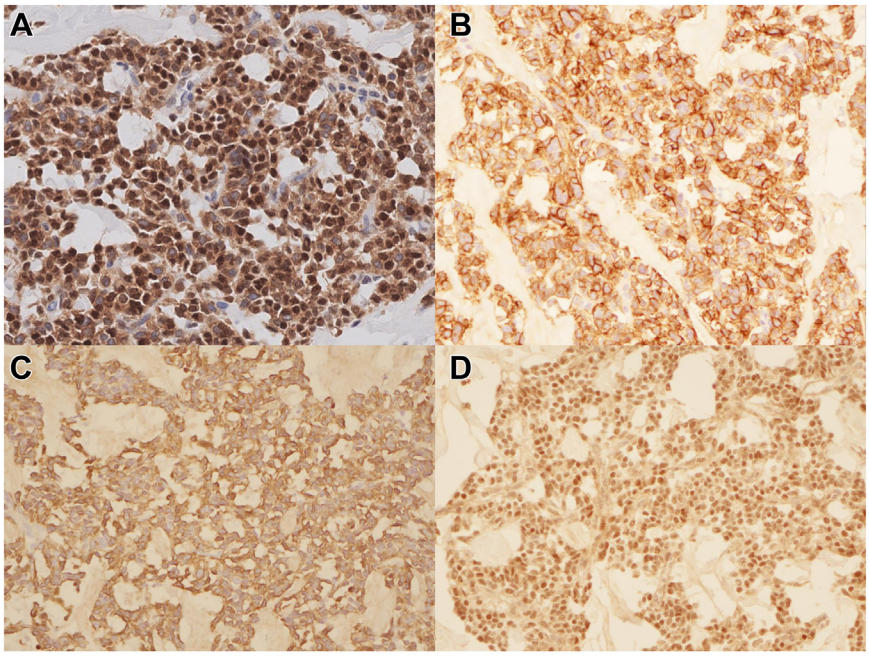

Figure 2.
Immunohistochemical staining results of *GLI1*-altered mesenchymal tumors. They are frequently positive for (A) GLI1 and (B) CD56. (C) A few cases are also positive for SMA. (D) A case in our cohort (case 2) is positive for BCOR, which leads to initial misdiagnosis of sarcoma with *BCOR* genetic alterations.

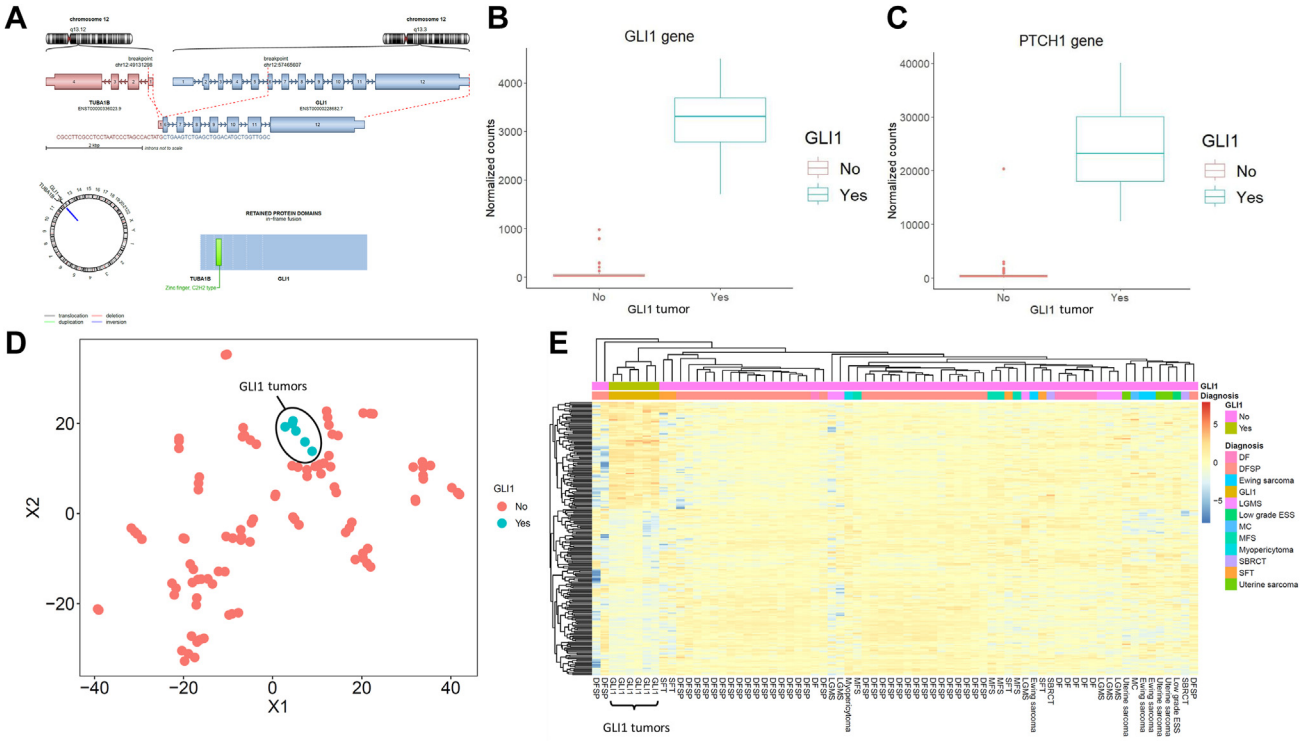

Figure 3.
RNA-seq analysis. (A) A novel fusion partner *TUBA1B* was detected, involving exon 1 of *TUBA1B* and exon 6 of *GLI1*. Differential gene expression analysis revealed upregulation of (B) *GLI1* and (C) *PTCH1* genes of *GLI1*-altered mesenchymal tumors. Unsupervised clustering analysis using (D) t-distributed stochastic neighbor embedding plot and (E) hierarchical clustering showed distinct expression profile of GLI1-altered mesenchymal tumors. DF, dermatofibroma; DFSP, dermatofibrosarcoma protuberans; ESS, endometrial stromal sarcoma; LGMS, low-grade myofibroblastic sarcoma; MC, mesenchymal chondrosarcoma; MFS, myxofibrosarcoma; SBRCT, small blue round cell tumor; SFT, solitary fibrous tumor.

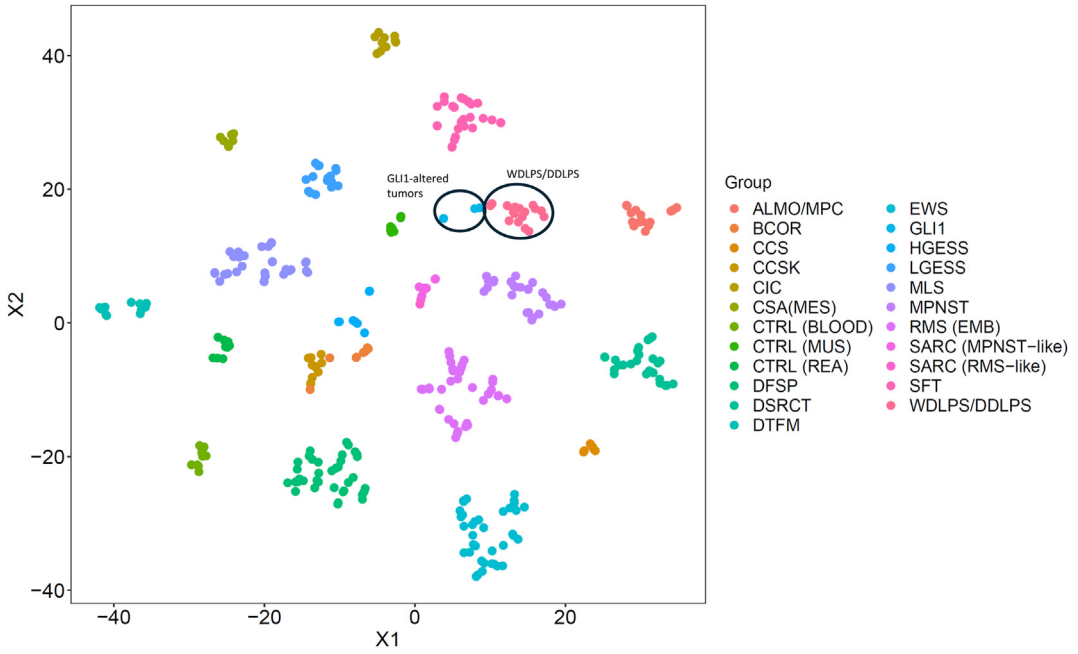

Figure 4.
Methylation EPIC analysis. Unsupervised clustering analysis using t-distributed stochastic neighbor embedding plot revealed *GLI1*-altered mesenchymal tumors forming a distinct cluster among other entities in the differential diagnosis. ALMO, angioleiomyoma; BCOR, sarcoma with BCOR genetic alteration; CCS, clear cell sarcoma; CCSK, clear cell sarcoma of kidney; CIC, sarcoma with CIC genetic alteration; CSA (MES), mesenchymal chondrosarcoma; CTRL, control; DDLPS, dedifferentiated liposarcoma; DFSP, dermatofibrosarcoma protuberans; DSRCT, desmoplastic small round cell tumor; DTFM, desmoid-type fibromatosis; EWS, Ewing sarcoma; HGESS, high-grade endometrial stromal sarcoma; LGESS, low-grade endometrial stromal sarcoma; MLS, myxoid liposarcoma; MPC, myopericytoma; MPNST, malignant peripheral nerve sheath tumor; MUS, muscle; REA, reactive tissue; RMS, rhabdomyosarcoma; SFT, solitary fibrous tumor; WDLPS, well-differentiated liposarcoma.

Table 2
Comparison of clinicopathologic features of *GLI1* fusion and *GLI1*-amplified tumors

Clinicopathological factors	Fusion (n = 108)	Amplification (n = 53)	*P*
Age, median (range) (y)	40.5 (0-84)	46 (1-88)	.84
Sex			.179
Female	46 (42.6)	29 (54.7)	
Male	62 (57.4)	24 (45.3)	
Size, median (range) (cm)	4.5 (0.8-21.2)	1.7 (0.6-12)	<.001[a]
Site			<.001[a]
Extremities	25 (23.8)	24 (45.3)	
Head and neck	29 (27.6)	16 (30.2)	
Trunk	20 (19.0)	7 (13.2)	
Intraabdominal	23 (21.9)	1 (1.9)	
Pelvis	7 (6.7)	2 (3.8)	
Intrathoracic	1 (1)	2 (3.8)	
Intracranial	0 (0)	1 (1.9)	
Mitotic index, median (range) (mitoses/10 HPFs)	1 (0-40)	5 (0-34)	<.001[a]
Necrosis			.112
Absent	83 (86.5)	39 (75)	
Present	13 (13.5)	13 (25)	
Local recurrence, n (%)			.132
No	65 (86.7)	19 (73.1)	
Yes	10 (13.3)	7 (26.9)	
Metastasis, n (%)			.797
No	51 (72.9)	20 (76.9)	
Yes	19 (27.1)	6 (23.1)	
Death, n (%)			1
No	72 (94.7)	29 (93.5)	
Yes	4 (5.3)	2 (6.5)	

HPF, high-power field.
[a] Statistically significant ($P < .05$).

significant prognostic difference in terms of local recurrence, metastasis, and death. Survival comparative studies showed that *GLI1*-amplified tumors had significantly worse overall survival ($P = .017$) compared with the *GLI1*-rearranged counterpart, but there is no significant difference in progression-free survival ($P = .4$) (Supplementary Fig. S2).

Additionally, we investigated which clinicopathologic features are predictive of metastasis for *GLI1*-altered mesenchymal tumors. We found that size ≥6 cm and mitotic count ≥5 per 10 HPFs are significantly associated with risk of metastasis in both univariate and multivariate analyses (Table 3). Age, sex, site, presence of necrosis, *GLI1* alteration type, fusion partners, and *GLI1* fusion location are not predicting malignant behaviors. We grouped tumors having both ≥ 6 cm size and mitotic count ≥5 per 10 HPFs as high risk and other cases as low risk, and we demonstrated that high-risk tumors had both significantly worse overall survival ($P < .001$) and disease-free survival ($P < .0001$) (Fig. 5). Tumors located at superficial sites might have intrinsically better prognosis because of ease of complete surgical excision, and therefore, we did all the above analyses separately excluding tumors in superficial location. We found similar results, and the risk stratification system still demonstrated stratifying power in both overall survival and progression-free survival (Supplementary Fig. S3, Supplementary Tables S2 and S3).

Discussion

GLI1-altered mesenchymal tumors represent an emerging molecularly defined group of tumors characterized by either *GLI1* fusion or amplification. Originally described to be found predominantly in the H&N regions, they were subsequently found in much wider anatomical locations, such as the trunk and extremities, gastrointestinal tract, and genitourinary tract. In our combined analysis of all the reported cases, trunk and extremities actually represented the most common sites (48.8%), with H&N regions being the second most common location (28.1%). There was a wide range of presentation age (from congenital to 88 years old) with no particular sex predilection (M:F ratio, 1.17:1). Microscopically, they usually exhibited a multinodular, lobulated, or plexiform architecture frequently separated by thick fibrous bands. They were composed of monomorphic ovoid to round or vaguely epithelioid cells arranged in compact or ill-defined nests interspersed with rich arborizing capillary network. This morphologic pattern had also been designated as “distinctive nested glomoid neoplasms.”[38] Perivascular aggregates of tumor cells protruding into dilated vascular spaces were frequently seen, mimicking lymphovascular invasion. Other features that may be observed included cystic changes and myxoid areas. The presence of abundant multinucleated giant cells was also recently reported in another series.[50]

The IHC profile of *GLI1*-altered mesenchymal tumors is variable and relatively nonspecific. Our study confirms the sensitivity of GLI1 IHC in the workup of *GLI1*-altered mesenchymal tumors. GLI1 IHC was diffusely positive in all cases tested with strong staining intensity. It was described to have a sensitivity of 91.3% and specificity of 98%.[51] Another highly sensitive marker is CD56, which was positive in >90% of reported cases tested. Obviously, it is highly nonspecific, which can be seen positive in neuroendocrine tumors, ovarian sex cord-stromal tumors, and natural killer cells, among others. A subset of cases was also positive for S100 (43%) and SMA (32.8%), but SOX10 was typically negative. Stainings with cytokeratins by AE1/3 may be positive, mainly in a patchy pattern for approximately 30% cases, but CAM5.2 was mainly negative. Intriguely, CD10 and cyclin D1 were positive in nearly all cases tested, mainly in those in the female genital tracts.

GLI1-altered mesenchymal tumors have been intrinsically defined by molecular changes of the *GLI1* gene, but it is uncertain whether they should represent a molecularly defined entity, or they actually represent a known entity defined by morphology and IHC staining profile with *GLI1* gene alterations. To address this question, we try to perform multiomics analysis of this group of tumor. Interestingly, despite being located at different sites with a slightly different morphology, *GLI1*-altered mesenchymal tumors feature a distinct expression and epigenomic profile well separated from other tumors. Specifically, among tumors that may fall into morphologic differential diagnosis, such as various round cell sarcomas (eg, Ewing sarcoma, *CIC*-translocated sarcoma, and *BCOR*-rearranged sarcoma), myopericytoma, and angioleiomyoma, they form a recognizable epigenomics cluster. Similar observations are seen for entities that may share similar ancillary test findings because of alteration of genes next to the *GLI1* gene, including well-differentiated liposarcoma and dedifferentiated liposarcoma characterized by *MDM2* gene amplification and solitary fibrous tumors featured by STAT6 expression. As expected, the expression of *GLI1* gene and its effectors genes is also overexpressed, thus forming a distinct expression profile and cluster. These findings suggest *GLI1*-altered mesenchymal tumors may represent a separate entity defined by *GLI1* gene alteration with distinctive clinicopathologic and molecular features.

Recurrent *GLI1* fusions have also been identified in 2 unique types of gastric tumors: plexiform fibromyxoma and gastroblastoma.[52,53] Plexiform fibromyxoma is a benign neoplasm that typically originates in the antrum or pyloric region, displaying a multinodular and plexiform architecture with uniform spindle cell

Table 3
Univariate and multivariate analyses of different clinicopathologic features predicting metastasis

Clinicopathological factors	Metastasis, n (%)		Univariate, OR (95% CI)	*P*	Multivariate, OR (95% CI)	*P*
	No	Yes				
Age (y)				.833		
<40	35 (74.5)	12 (25.5)	1.000 (reference)			
≥40	37 (74)	13 (26)	1.025 (0.411-2.572)			
Sex				.321		
Female	32 (69.6)	14 (30.4)	1.000 (reference)			
Male	40 (78.4)	11 (21.6)	0.629 (0.247-1.566)			
Size (cm)				.003[a]	5.226 (1.185-26.662)	.033[a]
<6	45 (88.2)	6 (11.8)	1.000 (reference)			
≥6	14 (56.0)	11 (44.0)	5.893 (1.902-19.976)			
Site						
Extremities and trunk	31 (72.1)	12 (27.9)	1.000 (reference)			
Head and neck	17 (77.3)	5 (22.7)	0.760 (0.212-2.434)	.653		
Internal organs	22 (75.9)	7 (24.1)	0.822 (0.268-2.386)	.722		
Mitotic count				<.001[a]	10.656 (2.288-61.681)	.004[a]
<5/10 HPFs	48 (85.7)	8 (14.3)	1.000 (reference)			
≥5/10 HPFs	10 (40)	15 (60)	9.000 (3.114-28.335)			
Necrosis				.004[a]	0.892 (0.126-5.125)	.903
Absent	50 (78.1)	14 (21.9)	1.000 (reference)			
Present	10 (47.6)	11 (52.4)	4.007 (1.424-11.610)			
GLI1 alteration type				.983		
Amplification	19 (73.1)	7 (26.9)	1.000 (reference)			
Fusion	51 (72.9)	19 (27.1)	1.011 (0.376-2.931)			
Fusion partner						
ACTB	28 (70.0)	12 (30.0)	1.000 (reference)			
MALAT1	4 (80.0)	1 (20.0)	0.583 (0.028-4.479)	.645		
PTCH1	4 (66.67)	2 (33.3)	1.167 (0.147-6.862)	.869		
Others	14 (87.5)	2 (12.5)	0.333 (0.048-1.449)	.186		
GLI1 fusion location						
Exon 5	6 (85.7)	1 (14.3)	1.000 (reference)			
Exon 6	21 (77.7)	6 (22.2)	1.714 (0.225-35.670)	.646		
Exon 7	3 (50.0)	3 (50.0)	6.000 (0.511-155.194)	.186		
Others	19 (73.1)	7 (26.9)	2.667 (0.366-54.729)	.398		

HPF, high-power field; OR, odds ratio.
[a] Statistically significant ($P < .05$).

morphology and SMA positivity. These tumors often contain *MALAT1::GLI1* fusions. Despite sharing morphologic and IHC similarities with other *GLI1*-altered mesenchymal tumors, they are currently considered a distinct clinicopathologic entity. Conversely, gastroblastoma is a malignant tumor that predominantly presents in the gastric antrum and is more common in men. These tumors also exhibit recurrent *MALAT1::GLI1* fusions.[52] They are characterized by a biphasic proliferation of uniform spindle cells and nested

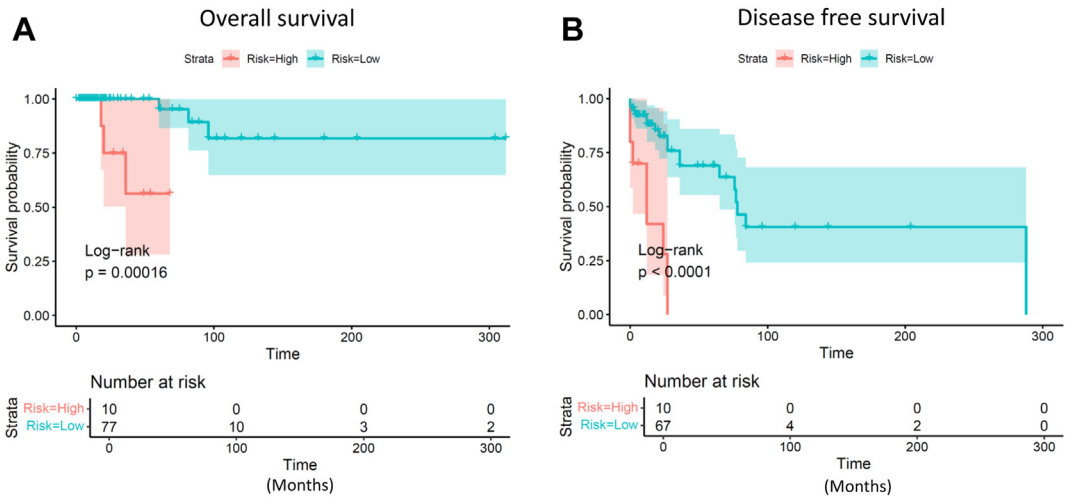

Figure 5.
Kaplan-Meier survival curves for *GLI1*-altered mesenchymal tumors, stratified based on the presence of both high-risk features: mitotic count ≥5 per 10 high-power fields and size ≥6 cm. (A) Overall survival, log-rank test, $P = .0016$. (B) Disease-free survival, log-rank test, $P < .0001$. Shaded regions indicate 95% CIs.

epithelial cells. Unlike other *GLI1*-altered mesenchymal tumors, gastroblastomas characteristically express keratins, emphasizing the epithelial component. Owing to their distinctive clinicopathologic features, gastroblastomas are classified as a separate entity from other *GLI1*-altered mesenchymal tumors.

In the combined appraisal of all cases of *GLI1*-altered mesenchymal tumors in the literature and together with our case series, we investigated if there were any clinicopathologic differences between tumors with *GLI1* fusion and *GLI1* amplification. Compared with *GLI1* fusion tumors, *GLI1*-amplified tumors were identified in a smaller size, were more commonly located in the extremities, and had a higher mitotic index. However, there was no significant prognostic difference in terms of local recurrence, metastasis, and death. In contrast, there was a significant difference in overall survival but not disease-free survival, similar to what was reported recently by Saoud et al.[50]

Although there is clear evidence of metastatic potential from different case reports and series, the clinicopathologic features predicting malignant behavior are currently unknown. Given the relatively small number of cases in the literature, it has been challenging to identify prognostic factors for *GLI1*-altered mesenchymal tumors. Combining our cohort of 6 cases of *GLI1*-altered mesenchymal tumors with a comprehensive literature review, we analyzed a total of 167 cases for different clinicopathologic features for association with prognosis. By pooling the clinicopathologic factors and outcomes of published cases, we were able to identify the prognostic factors of size and mitotic index to predict metastasis. Overall, there were 25.8% cases featuring metastasis. Univariate and multivariate logistic regression analyses identified a size of $\geq$6 cm and mitotic count of $\geq$5 per 10 HPFs as significant prognostic factors predictive of metastasis. By classifying tumors as high risk based on the presence of both increased size ($\geq$6 cm) and mitotic activity ($\geq$5/10 HPFs), we demonstrated that *GLI1*-altered mesenchymal tumors can be risk stratified with a significant survival difference. These 2 parameters are generally applicable to most other tumors, which have been incorporated in TNM staging or other risk stratification system. Although the precise criteria used for prognostication of *GLI1*-altered mesenchymal tumors will inevitably be further refined as additional cases are reported, we believe this provides an early framework for predicting behavior based on clinicopathologic features. Ultimately, recognizing *GLI1*-altered mesenchymal tumors and using targeted therapy can significantly improve patient outcomes,[54] and the risk stratification system can pave the way to select high-risk patients for personalized effective treatments in the future.

Limitations

Although pooling outcome data from many different series allowed us to identify potential prognostic features, this approach also introduced several inherent limitations. Specifically, the type and extent of tumor necrosis were not incorporated in the model; the field diameter used for mitotic counts was not standardized, and the recording of atypia was subjective and therefore not included in the analysis. Furthermore, there is significant interobserver variability in the counting of mitotic figures, and because mitotic counts were abstracted from different studies, the values used in our analysis are inherently inaccurate.

Finally, the number of cases for clustering analysis may be too few to deduce a concrete conclusion, and we do not have samples of gastroblastoma and plexiform fibromyxoma for comparison. Further study involving a larger number of samples will be warranted to elucidate the best classification of this group of tumors.

Author Contributions

M.C.F.Y. and T.W.H.S. performed study concept and design. M.C.F.Y. performed a comprehensive literature review and data retrieval, multiomics analysis, and statistical analysis and participated in writing of manuscript. M.C.F.Y. and A.P.Y.L. performed interpretation of data. M.C.F.Y., A.P.Y.L., S.-I.W., and H.H.L. collected data of local cohort. All authors read and approved the final paper.

Data Availability

The data supporting the findings of this study are available within the article and its supplementary materials or from the corresponding author upon reasonable request.

Funding

This work was supported by Health and Medical Research Fund (Commissioned Paediatric Research at the Hong Kong Children's Hospital, PR-HKU-6), Food and Health Bureau, Hong Kong SAR Government.

Declaration of Competing Interest

The authors report no relevant conflicts of interest.

Ethics Approval and Consent to Participate

The study was approved by local institutional review board (UW22-168) and the need of patient's consent was waived due to retrospective nature of the study.

Supplementary Material

The online version contains supplementary material available at https://doi.org/10.1016/j.modpat.2024.100635.

References

1. Haas BJ, Dobin A, Li B, Stransky N, Pochet N, Regev A. Accuracy assessment of fusion transcript detection via read-mapping and de novo fusion transcript assembly-based methods. *Genome Biol*. 2019;20(1):213.
2. Uhrig S, Ellermann J, Walther T, et al. Accurate and efficient detection of gene fusions from RNA sequencing data. *Genome Res*. 2021;31(3):448–460.
3. Love MI, Huber W, Anders S. Moderated estimation of fold change and dispersion for RNA-seq data with DESeq2. *Genome Biol*. 2014;15(12):550.
4. Li H, Durbin R. Fast and accurate short read alignment with Burrows–Wheeler transform. *Bioinformatics*. 2009;25(14):1754–1760.
5. McKenna A, Hanna M, Banks E, et al. The Genome Analysis Toolkit: a MapReduce framework for analyzing next-generation DNA sequencing data. *Genome Res*. 2010;20(9):1297–1303.
6. Wang K, Li M, Hakonarson H. ANNOVAR: functional annotation of genetic variants from high-throughput sequencing data. *Nucleic Acids Res*. 2010;38(16), e164.
7. Li MM, Datto M, Duncavage EJ, et al. Standards and guidelines for the interpretation and reporting of sequence variants in cancer: a joint consensus recommendation of the Association for Molecular Pathology, American Society of Clinical Oncology, and College of American Pathologists. *J Mol Diagn*. 2017;19(1):4–23.
8. Jia P, Yang X, Guo L, et al. MSIsensor-pro: fast, accurate, and matched-normal-sample-free detection of microsatellite instability. *Genomics Proteomics Bioinformatics*. 2020;18(1):65–71.
9. Mayakonda A, Lin D-C, Assenov Y, Plass C, Koeffler HP. Maftools: efficient and comprehensive analysis of somatic variants in cancer. *Genome Res*. 2018;28(11):1747–1756.

10. Aryee MJ, Jaffe AE, Corrada-Bravo H, et al. Minfi: a flexible and comprehensive Bioconductor package for the analysis of Infinium DNA methylation microarrays. *Bioinformatics*. 2014;30(10):1363–1369. https://doi.org/10.1093/bioinformatics/btu049
11. Koelsche C, Schrimpf D, Stichel D, et al. Sarcoma classification by DNA methylation profiling. *Nat Commun*. 2021;12(1):498.
12. Sharma AE, Dickson M, Singer S, Hameed MR, Agaram NP. GLI1 coamplification in well-differentiated/dedifferentiated liposarcomas: clinicopathologic and molecular analysis of 92 cases. *Mod Pathol*. 2024;37(6), 100494.
13. Agaram NP, Zhang L, Sung Y-S, et al. GLI1-amplifications expand the spectrum of soft tissue neoplasms defined by GLI1 gene fusions. *Mod Pathol*. 2019;32(11):1617–1626.
14. Aivazian K, Mahar A, Jackett LA, Kimble RM, Scolyer RA. GLI activated epithelioid cell tumour: report of a case and proposed new terminology. *Pathology*. 2021;53(2):267–270.
15. Alwaqfi RR, Samuelson MI, Guseva NN, Ouyang M, Bossler AD, Ma D. PTCH1-GLI1 fusion-positive ovarian tumor: report of a unique case with response to tyrosine kinase inhibitor pazopanib. *J Natl Compr Canc Netw*. 2021;19(9):998–1004.
16. Ambrosio M, Virgilio A, Raffone A, et al. Malignant epithelioid neoplasm of the ileum with ACTB-GLI1 fusion mimicking an adnexal mass. *BMC Womens Health*. 2022;22(1):104.
17. Antonescu CR, Agaram NP, Sung Y-S, Zhang L, Swanson D, Dickson BC. A distinct malignant epithelioid neoplasm with GLI1 gene rearrangements, frequent S100 protein expression, and metastatic potential: expanding the spectrum of pathologic entities with ACTB/MALAT1/PTCH1-GLI1 fusions. *Am J Surg Pathol*. 2018;42(4):553–560.
18. Argani P, Boyraz B, Oliva E, et al. GLI1 gene alterations in neoplasms of the genitourinary and gynecologic tract. *Am J Surg Pathol*. 2022;46(5):677–687.
19. Bridge JA, Sanders K, Huang D, et al. Pericytoma with t(7;12) and ACTB-GLI1 fusion arising in bone. *Hum Pathol*. 2012;43(9):1524–1529.
20. Castro E, Cortes-Santiago N, Ferguson LMS, Rao PH, Venkatramani R, López-Terrada D. Translocation t(7;12) as the sole chromosomal abnormality resulting in ACTB-GLI1 fusion in pediatric gastric pericytoma. *Hum Pathol*. 2016;53:137–141.
21. Dahlén A, Fletcher CDM, Mertens F, et al. Activation of the GLI oncogene through fusion with the beta-actin gene (ACTB) in a group of distinctive pericytic neoplasms: pericytoma with t(7;12). *Am J Pathol*. 2004;164(5):1645–1653.
22. Dahlén A, Mertens F, Mandahl N, Panagopoulos I. Molecular genetic characterization of the genomic ACTB-GLI fusion in pericytoma with t(7;12). *Biochem Biophys Res Commun*. 2004;325(4):1318–1323.
23. Hui L, Bai Q, Yang W, et al. GLI1-rearranged mesenchymal tumor in the ovary. *Histopathology*. 2022;81(5):688–692.
24. Ichikawa D, Yamashita K, Okuno Y, et al. Integrated diagnosis based on transcriptome analysis in suspected pediatric sarcomas. *NPJ Genom Med*. 2021;6(1):49.
25. Jessurun J, Orr C, McNulty SN, et al. GLI1 -rearranged enteric tumor: expanding the spectrum of gastrointestinal neoplasms with GLI1 gene fusions. *Am J Surg Pathol*. 2023;47(1):65–73.
26. Kerr DA, Cloutier JM, Margolis M, et al. GLI1-altered mesenchymal tumors with ACTB or PTCH1 fusion: a molecular and clinicopathologic analysis. *Mod Pathol*. 2024;37(2):100386.
27. Kerr DA, Pinto A, Subhawong TK, et al. Pericytoma with t(7;12) and ACTB-GLI1 fusion: reevaluation of an unusual entity and its relationship to the spectrum of GLI1 fusion-related neoplasms. *Am J Surg Pathol*. 2019;43(12):1682–1692.
28. Khan MA, Maharaj K, Burns C, Cameron M. A rare case of a GLI1-ACTB-rearranged mesenchymal tumor of the tongue in an 8-year-old boy. *J Oral Maxillofac Surg*. 2021;79(10):e93–e94.
29. Klubíčková N, Kinkor Z, Michal M, et al. Epithelioid soft tissue neoplasm of the soft palate with a PTCH1-GLI1 fusion: a case report and review of the literature. *Head Neck Pathol*. 2022;16(2):621–630.
30. Koh NWC, Seow WY, Lee YT, Lam JCM, Lian DWQ. Pericytoma with t(7;12): the first ovarian case reported and a review of the literature. *Int J Gynecol Pathol*. 2019;38(5):479–484.
31. Liu J, Mao R, Lao IW, et al. GLI1-altered mesenchymal tumor: a clinicopathological and molecular analysis of ten additional cases of an emerging entity. *Virchows Arch*. 2022;480(5):1087–1099.
32. Lopez-Nunez O, Surrey LF, Alaggio R, Herradura A, McGough RL, John I. Novel APOD-GLI1 rearrangement in a sarcoma of unknown lineage. *Histopathology*. 2021;78(2):338–340.
33. Machado I, Hosler GA, Traves V, et al. Superficial GLI1-amplified mesenchymal neoplasms: expanding the spectrum of an emerging entity which reaches the realm of dermatopathology. *J Cutan Pathol*. 2023;50(6):487–499.
34. Mendelson NL, Al Assaad M, Hadi K, et al. Whole-genome analysis elucidates complex genomic events in GLI1 -rearranged enteric tumor. *Am J Surg Pathol*. 2023;47(10):1192–1193.
35. Nitta Y, Takeda M, Fujii T, et al. A case of pericytic neoplasm in the shoulder with a novel DERA-GLI1 gene fusion. *Histopathology*. 2021;78(3):466–469.
36. Palsgrove DN, Rooper LM, Stevens TM, et al. GLI1-altered soft tissue tumors of the head and neck: frequent oropharyngeal involvement, p16 immunoreactivity, and detectable alterations by DDIT3 break apart FISH. *Head Neck Pathol*. 2022;16(4):1146–1156.
37. Panagopoulos I, Gorunova L, Rise TV, Andersen K, Micci F, Heim S. An unbalanced chromosome translocation between 7p22 and 12q13 leads to ACTB-GLI1 fusion in pericytoma. *Anticancer Res*. 2020;40(3):1239–1245.
38. Papke DJ Jr, Dickson BC, Oliveira AM, Sholl LM, Fletcher CDM. Distinctive nested glomoid neoplasm: clinicopathologic analysis of 20 cases of a mesenchymal neoplasm with frequent GLI1 alterations and indolent behavior. *Am J Surg Pathol*. 2023;47(1):12–24.
39. Pettus JR, Kerr DA, Stan RV, et al. Primary myxoid and epithelioid mesenchymal tumor of the kidney with a novel GLI1-FOXO4 fusion. *Genes Chromosomes Cancer*. 2021;60(2):116–122.
40. Prall OWJ, McEvoy CRE, Byrne DJ, et al. A malignant neoplasm from the jejunum with a MALAT1-GLI1 fusion and 26-year survival history. *Int J Surg Pathol*. 2020;28(5):553–562.
41. Punjabi LS, Goh CHR, Sittampalam K. Expanding the spectrum of GLI1-altered mesenchymal tumors—a high-grade uterine sarcoma harboring a novel PAMR1::GLI1 fusion and literature review of GLI1-altered mesenchymal neoplasms of the gynecologic tract. *Genes Chromosomes Cancer*. 2023;62(2):107–114.
42. Rollins BT, Cassarino DS, Lindberg M. Primary cutaneous epithelioid mesenchymal neoplasm with ACTB-GLI1 fusion: a case report. *J Cutan Pathol*. 2022;49(3):284–287.
43. Shahabi A, Israel A-K, Sullivan CB, McHugh KE. Fine needle aspiration biopsy of epithelioid-mesenchymal neoplasm with PTCH1-GLI1 fusion: a case report. *Diagn Cytopathol*. 2022;50(8):E223–E229.
44. Xu B, Chang K, Folpe AL, et al. Head and neck mesenchymal neoplasms with GLI1 gene alterations: a pathologic entity with distinct histologic features and potential for distant metastasis. *Am J Surg Pathol*. 2020;44(6):729–737.
45. Zeng Y, Yao H, Jiang X, Tang X, Wang X. GLI1-altered mesenchymal tumor involving the duodenum: case report and literature review. *Int J Surg Pathol*. 2023;31(8):1538–1547.
46. Zhong H, Xu C, Chen X, Guo X, Yang S. GLI1-altered epithelioid soft tissue tumor: a newly described entity with a predilection for the tongue. *Oral Surg Oral Med Oral Pathol Oral Radiol*. 2022;134(1):e14–e22.
47. Liu YJ, Wagner MJ, Kim EY, Chen EY. TUBA1A-GLI1 fusion in a soft tissue myoepithelial neoplasm. *Hum Pathol Case Rep*. 2021;24, 200497.
48. Li J, Zuo L, Tang L, Yan X, Chen S. Duodenal soft tissue sarcoma with GLI1 gene rearrangement: a case report and literature review. *Am J Case Rep*. 2024;25, e943271.
49. Machado I, Agaimy A, Giner F, et al. The value of GLI1 and p16 immunohistochemistry in the premolecular screening for GLI1-altered mesenchymal neoplasms. *Virchows Arch*. 2024;484(5):765–775.
50. Saoud C, Agaimy A, Dermawan JK, et al. A comprehensive clinicopathologic and molecular reappraisal of GLI1-altered mesenchymal tumors with pooled outcome analysis showing poor survival in GLI1- amplified versus GLI1-rearranged tumors. *Am J Surg Pathol*. 2024;48(10):1302–1317.
51. Parrack PH, Mariño-Enríquez A, Fletcher CDM, Hornick JL, Papke Jr DJ. GLI1 immunohistochemistry distinguishes mesenchymal neoplasms with GLI1 alterations from morphologic mimics. *Am J Surg Pathol*. 2023;47(4):453–460.
52. Graham RP, Nair AA, Davila JI, et al. Gastroblastoma harbors a recurrent somatic MALAT1-GLI1 fusion gene. *Mod Pathol*. 2017;30(10):1443–1452.
53. Spans L, Fletcher CDM, Antonescu CR, et al. Recurrent MALAT1-GLI1 oncogenic fusion and GLI1 up-regulation define a subset of plexiform fibromyxoma. *J Pathol*. 2016;239(3):335–343.
54. Avery JT, Zhang R, Boohaker RJ. GLI1: a therapeutic target for cancer. *Front Oncol*. 2021;11:673154.